DETECTION OF CFRP COMPOSITE MANUFACTURING DEFECTS USING A GUIDED WAVE APPROACH*

Tyler B. Hudson[1,2], Tan-Hung Hou[3], Brian W.Grimsley[3], Fuh-Gwo Yuan[1,2]
[1] Department of Mechanical and Aerospace Engineering
North Carolina State University
Raleigh, NC 27695
[2] National Institute of Aerospace
Hampton, VA 23666
[3] NASA Langley Research Center, Advanced Materials and Processing Branch
Hampton, VA 23681

ABSTRACT

NASA Langley Research Center is investigating a guided wave-based defect detection technique for as-fabricated carbon fiber reinforced polymer (CFRP) composites. This technique will be extended to perform in-process cure monitoring, defect detection and size determination, and ultimately a closed-loop process control to maximize composite part quality and consistency. The overall objective of this work is to determine the capability and limitations of the proposed defect detection technique, as well as the number and types of sensors needed to identify the size, type, and location of the predominant types of manufacturing defects associated with laminate layup and cure. This includes, porosity, gaps, overlaps, through-the-thickness fiber waviness, and in-plane fiber waviness. The present study focuses on detection of the porosity formed from variations in the matrix curing process, and on local overlaps intentionally introduced during layup of the prepreg.

By terminating the cure cycle prematurely, three 24-ply unidirectional composite panels were manufactured such that each subsequent panel had a higher final degree of cure, and lower level of porosity. It was demonstrated that the group velocity, normal to the fiber direction, of a guided wave mode increased by 5.52 percent from the first panel to the second panel and 1.26 percent from the second panel to the third panel. Therefore, group velocity was utilized as a metric for degree of cure and porosity measurements.

A fully non-contact guided wave hybrid system composed of an air-coupled transducer and a laser Doppler vibrometer (LDV) was used for the detection and size determination of an overlap. By transforming the plate response from the time-space domain to the frequency-wavenumber domain, the total wavefield was then separated into the incident and backscatter waves. The overlap region was accurately imaged by using a zero-lag cross-correlation (ZLCC) imaging condition, implying the incident and backscattered waves are in phase over the overlap boundaries.

1. INTRODUCTION

The NASA Advanced Composites Project seeks to develop and transition technology that will reduce the timeline required for development and certification of new aircraft structure that utilizes advanced composite materials. One area of concern is the formation of porosity and fiber waviness defects in composite structural parts during various processing stages, from incoming material

handling to the completion of laminate curing in an autoclave/vacuum press. Defects have detrimental effects on the quality of the structural parts, often leading to higher cost and significant delay in parts production and utilization.

In the composite industry, cure cycles are developed from a "trial and error" or a more effective "processing science" approach to reduce the final porosity level in the composite laminate [1]. Several studies have been published on the effects of porosity and their detection using non-destructive inspection techniques. Porosity is defined as "large number of microvoids each of which is too small to be of structural significance or to be detected individually by a realistic inspection technique, but which collectively may reduce the mechanical properties of the components to an unacceptable degree" [2]. Typically, porosity occurs because of entrapped air, moisture, or volatile products during the curing cycle [2]. In a special case with pure resins only, ultrasonic velocity has been used to infer the degree of cure because of its effect on the modulus of the resin [3-5]. In CFRP, it has been shown that as the porosity level increases, the ultrasonic velocity of the wave propagating perpendicular to the carbon fibers decreases [6]. Ultrasound can monitor end of cure based on when the time delay between the pulse and echo of the transducer plateaus (i.e. the ultrasonic velocity ceases to increase) in graphite/epoxy composites, [7] and epoxy matrices [8]. Non-contact, air-coupled transducers can be used for ultrasonic velocity measurement in resins when line of sight is available during curing [9]. Using mounted piezoceramic actuators and sensors can alleviate the unreliable coupling between an ultrasound transducer and the mold which can occur, especially during the phases of heating and cooling [10]. Other ultrasonic phenomena have also been used for monitoring degree of cure including attenuation [2,5-7,11], instantaneous phase, and the "mean value of each frequency curve weighted by the maximum corresponding spectral amplitude" [12].

Based on the premise that the level of porosity may be dictated by the change of the ultrasonic wave speed, this work examined the group velocity of guided waves in several panels with different final degrees of cure and lower level of porosity. The significance of this approach was that unlike conventional ultrasound that provides information about the quality of the part directly underneath or nearby the ultrasonic transducer in a point-by-point (discrete) inspection; the guided wave approach interrogated a continuous wave path through the thickness of the panel along the line from actuator to sensor. In addition, the experiment was designed such that it may be transitioned into a real-time detection system during cure. If the level of porosity can be estimated during curing, the cure cycle can be dynamically adjusted based on the measurements. This would prevent the operator from having to follow a prescribed, or non-optimized cure cycle.

Ply gaps and overlaps occur primarily at tow boundaries during the layup process and can lead to surface waviness [13]. Their effect on the ultimate strengths of composite laminates have been experimentally investigated [14]. Several optical imaging techniques have been or are being developed for the detection of gaps and overlaps during layup from an automated fiber placement (AFP) machine. The detection system can be manual or fully automated [13,15,16]. However, each of these systems cannot detect gaps and overlaps in a panel that has already been manufactured. Eddy currents have been used in a controlled research environment for the detection of gaps and overlaps on uncured prepreg [17].

For this study, the local defect detection and size determination for the overlap was devised by a fully non-contact laser ultrasound system based on a guided wave-based approach. The system was composed of a stationary air-coupled transducer, operating in the vicinity of the overlap region, and a laser Doppler vibrometer (LDV) that captured the wavefield by scanning the region.

Here, the total signal energy was first mapped in the region to show the area that was primarily illuminated by the air-coupled transducer. The wavefield, in time segments, in the illuminated region was then transformed into the frequency-wavenumber domain. In this domain, the incident and backscatter wavefield can be readily separated. Frequency-wavenumber filtering has previously been used for improved damage imaging of longitudinal slits in aluminum plates [18-20], disbonding in a composite wing [21], and delamination in a multi-layer composite plate [21]. The imaging metrics utilized were root mean square distribution of the reflected signal [18], cumulative standing wave energy [19], zero-lag cross-correlation (ZLCC) [20], standing wave filter [21], and Laplacian image filter [21]. For this work, the ZLCC imaging condition was utilized to reveal and image the overlap region.

2. EXPERIMENTATION

2.1 Porosity Detection

Three panels of twenty-four ply unidirectional Hexcel® IM7/8552 prepreg were fabricated in a vacuum press according to the cure cycles shown in Figure 1. The panels were 305 mm × 305 mm with nominal thickness of 3 mm. Each subsequent panel had a higher degree of cure than the previous one, based on the temperature and pressure experienced during the cure, also shown in Figure 1.

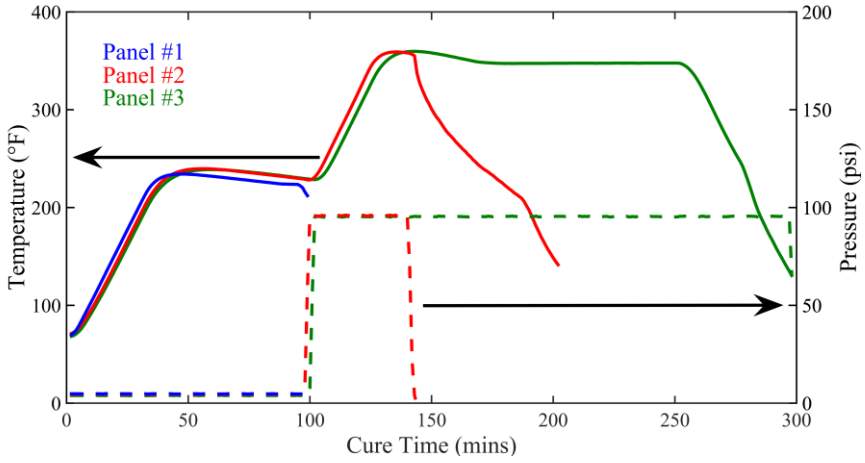

Figure 1. Cure cycle for Panel #1, #2, and #3.

After cure, each of the three panels were C-scanned (Figure 10) with a Sonix, Inc. immersion ultrasound system in pulse-echo mode using a Panametrics 15 MHz transducer. After C-scan, the panels were investigated by the guided wave approach. A guided wave was excited into the laminate using a five-peaked toneburst signal with a center frequency of 300 kHz emitted from a waveform generator (Agilent Technologies: 81150A) to an amplifier (Krohn-Hite Corporation: Model 7602M) to a piezoelectric disk (Steiner and Martins Inc.: SMD07T02R412WL). The laminate response was recorded by another piezoelectric disk in a pitch-catch configuration (Figure 2). To measure a wave propagating normal to the fiber direction (i.e., 90 degree direction), shown in Figure 3, each of the piezoelectric disks in the bottom row served as an actuator. The laminate response was recorded by the three piezoelectric disks along the same vertical column. This process was repeated for each of the four columns giving a total of twelve measurements.

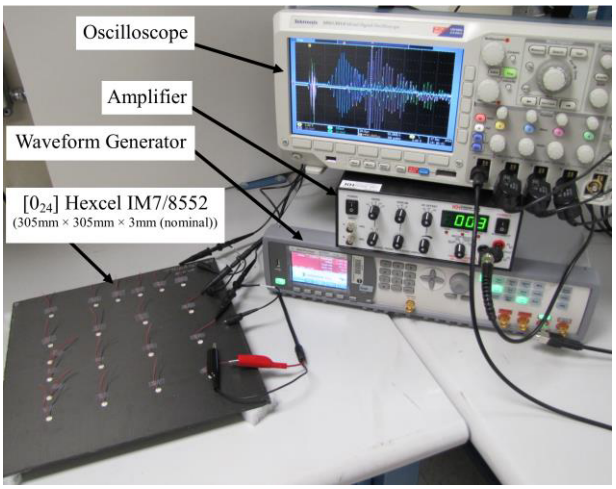

Figure 2. Experimental setup for detecting porosity level related to the ultrasonic wave velocity of a 24-ply unidirectional composite using piezolelectric disks.

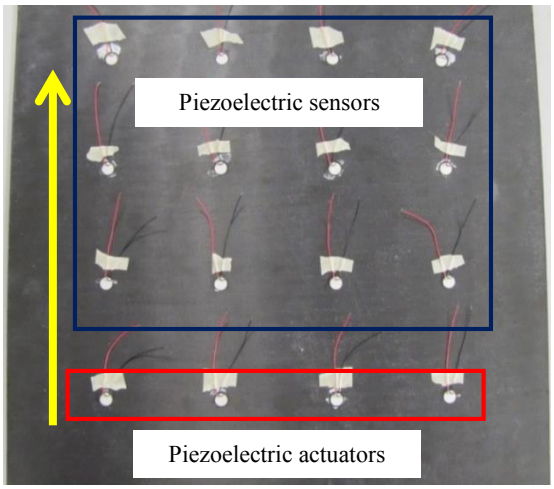

Figure 3. Actuation and sensing locations normal to the fiber (ninety degree) direction.

2.2 Overlap Detection

A panel was laid up by hand using Hexcel® IM7/8552 unidirectional prepreg. The layup was [0_4/90/90_2/90/0_4] where in the middle two layers overlap and gap defects were intentionally introduced. The entire panel was 150.4 mm × 150.4 mm × 1.524 mm (nominal) (6 in. × 6 in. × 0.06 in. (nominal)) and the overlap and the gap were of dimensions 63.5 mm × 6.35 mm × 0.25 mm (2.5 in × 0.25 in. × 0.01 in.) (Figure 4). The panel was cured in a vacuum press following the cure cycle recommended by Hexcel®. The temperature and pressure scheme for the cure cycle is similar to that of Panel #3 in Figure 1.

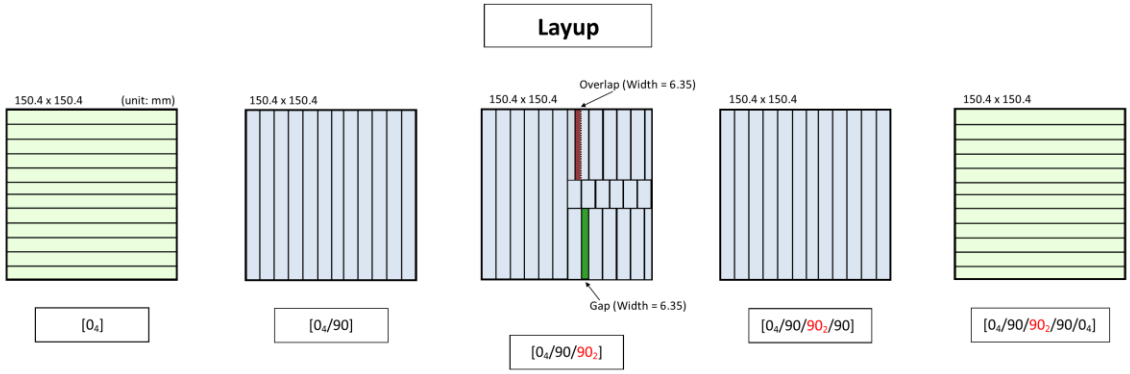

Figure 4. Layup of panel with intentionally introduced overlap and gap defects near the neutral ply surface of the composite laminate.

An unfocused circular air-coupled transducer with an active diameter of 25 mm (Ultran Group: NCG200-D25) was used to excite a five-peaked toneburst acoustic wave with a center frequency of 250 kHz (Figure 5). The excitation area on the plate was 26.5 mm × 25 mm. The location of the air-coupled transducer was stationary while the out-of-plane velocity of the A_0 Lamb wave was

recorded in a 1 mm × 1 mm grid inside the scan area (46 mm × 73 mm) (Figure 6) by a LDV (Polytec Inc.: OSV 500) (Figure 5).

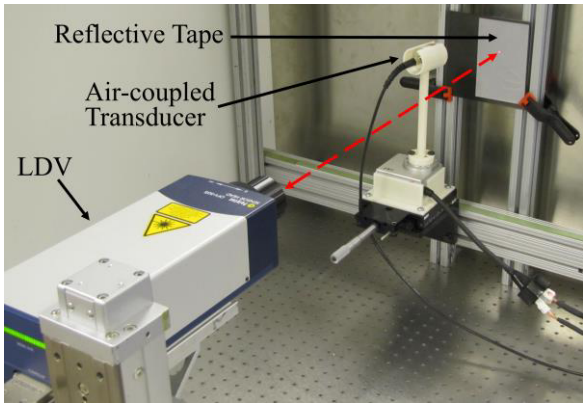

Figure 5. Experimental setup for detecting overlap region.

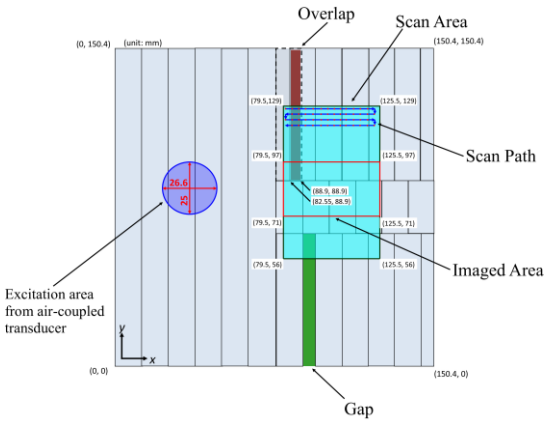

Figure 6. Excitation area from air-coupled transducer and LDV scan area (in blue) and imaged area (outlined by red rectangle).

3. RESULTS AND DISCUSSION

3.1 Porosity Detection

The group velocity of the guided wave, c_g, was calculated as the distance between the actuator and the sensor, d_{a-s}, divided by the time of flight (TOF) (Eq. (1))

$$c_g = \frac{d_{a-s}}{t_s - t_a} \tag{1}$$

where t_a is the time of actuation and t_s is the time of arrival at the sensor.

To determine t_a and t_s, the following algorithm was implemented. First, the time at which there is minimum response was determined and recorded as $t_{a(s)}\big|_{\min}$. Then, the time at the maximum peak prior to $t_{a(s)}\big|_{\min}$ was determined and recorded as $t_{a(s)}\big|_{\max}$. The reason $t_{a(s)}\big|_{\max}$ must be prior to $t_{a(s)}\big|_{\min}$ is that the asymmetric five-peaked toneburst signal generated is defined where the minimum value occurs after the maximum (Figure 7). $t_{a(s)}\big|_{\min}$ and $t_{a(s)}\big|_{\max}$ were checked to ensure that they occur on subsequent peaks by Eq. (2). If $t_{a(s)}\big|_{\min}$ and $t_{a(s)}\big|_{\max}$ did not satisfy Eq. (2), a secondary algorithm must be implemented to determine $t_{a(s)}\big|_{\max}$.

$$\frac{t_{a(s)}\big|_{\min} - t_{a(s)}\big|_{\max}}{N/f_c} \le 1 \tag{2}$$

where N equals the number of peaks (5) and f_c is the center frequency (300 kHz).

For each of the twelve measurements, $t_{a(s)}\big|_{\min}$ and $t_{a(s)}\big|_{\max}$ did satisfy Eq. (2). $t_{a(s)}$ was then calculated as the average of $t_{a(s)}\big|_{\min}$ and $t_{a(s)}\big|_{\max}$ (Eq. (3)).

$$t_{a(s)} = \frac{t_{a(s)}\big|_{\min} + t_{a(s)}\big|_{\max}}{2} \tag{3}$$

A plot of the actuation waveform and one of the sensor responses with the key time points in the algorithm is shown in Figure 7 and Figure 8, respectively.

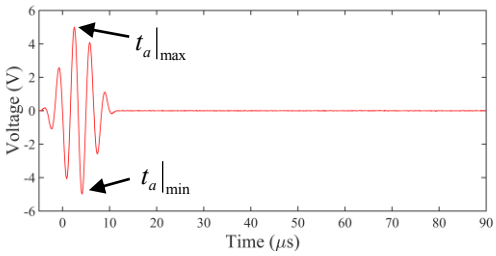

Figure 7. Actuation waveform.

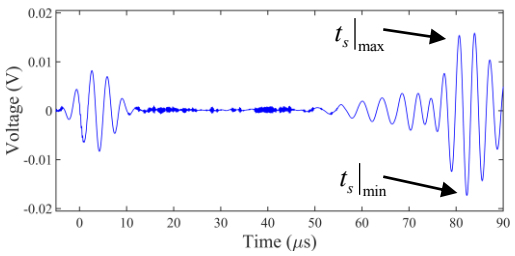

Figure 8. Plate response from sensor located five inches from actuator.

The average group velocity was then determined from the group velocities of each of the twelve actuator-sensor pairs. The three points in Figure 9 correspond to the average group velocity of each of the three panels. The cure time value is denoted by the time at which the composite panel began to cool during the curing cycle (Figure 1). The error bars show the variation based on a 90% confidence interval of the twelve measurements. The average group velocity increased by 5.52 percent from Panel #1 to Panel #2 and another 1.26 percent from Panel #2 to Panel #3 (Figure 9).

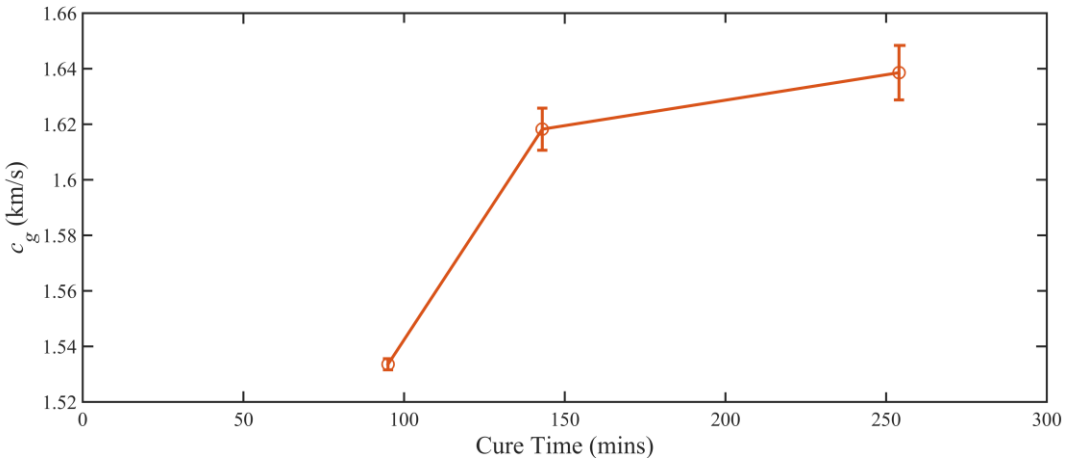

Figure 9. Group velocity normal to the fiber direction on each of three panels of varying final degrees of cure.

It is expected that each subsequent panel with longer cure times leads to a higher final degree of cure and lower porosity level. As shown in Figure 10, a decrease in the number of voids was

observed from each subsequent panel especially between Panel #1 and Panel #2. A lower porosity level in each subsequent panel can be confirmed from micrographs and/or acid digestion which were not completed at this time so that the panels could be utilized for future tests.

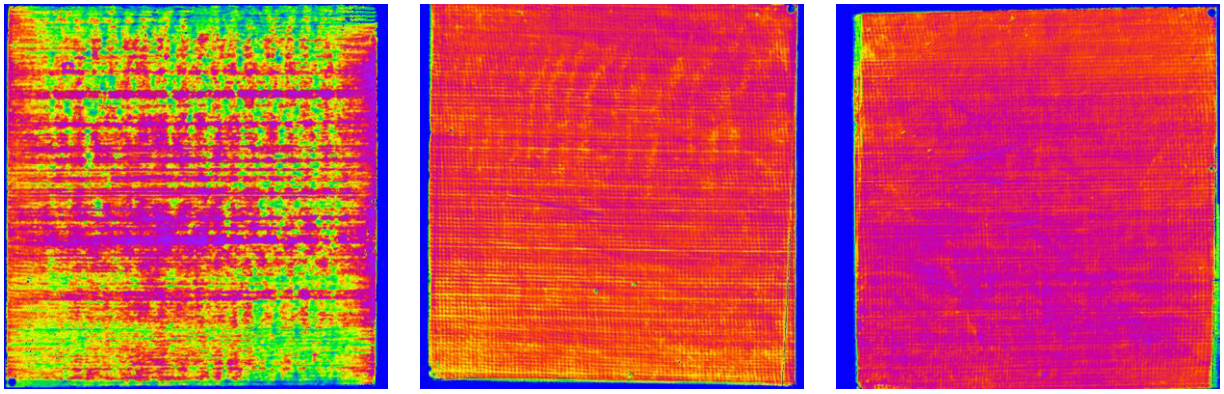

Panel #1 Panel #2 Panel #3

Figure 10. C-scan images of fabricated panels.

The average group velocity increased monotonically from Panel #1 to Panel #3. Therefore, preliminary results indicate that the group velocity of a guided wave could possibly be used as an initial index (or metric) to determine the degree of cure, and infer the level of porosity. This process can be transitioned into an in-line detection system that will be able to monitor the degree of cure and porosity in real-time within a part. The system will consist of high temperature actuators and sensors that can withstand the temperature and pressure during cure and high temperature cables that will connect the actuators and sensors to the electronics outside the cure environment. Many technical details will need to be determined to make this transition including mounting of the actuators and sensors to the mold, coupling the energy from the sensor to the part, and filtering out the effect of temperature on the signals.

3.2 Overlap Detection

After the panel was cured it was removed from the mold and C-scanned with the same system described in Section 2.1 to establish a baseline to compare with the guided wave approach (Figure 11).

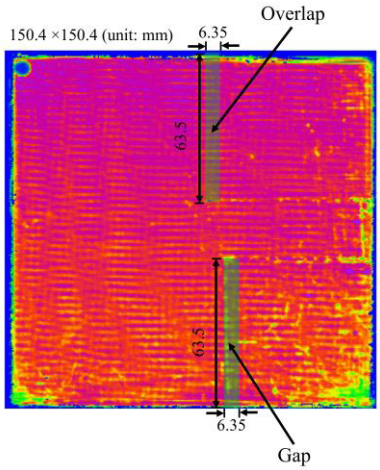

Figure 11. C-scan image of panel with intentionally introduced overlap and gap.

For the guided wave approach, the area that is to be imaged (46 mm × 26 mm) to reveal the overlap region in Figure 6 depends on the aperture of the air-coupled transducer. The angle of incidence of the air-coupled transducer was set to 13.5 degrees from normal. This value is optimized to ensure maximum amplitude of the desired mode of the propagating wave in the plate [22] and can be determined from the phase velocity dispersion curve (Figure 12).

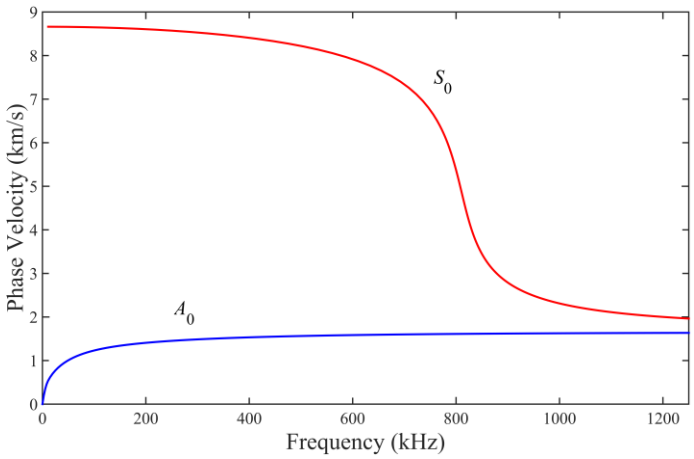

Figure 12. Phase velocity dispersion curve for the [0_4/90/90_2/90/0_4] composite plate.

At the center frequency of the excited wave (250 kHz), two fundamental wave modes simultaneously exist (A_0 and S_0). A_0 is the antisymmetric and S_0 is the symmetric zero-order Lamb wave mode. Since the magnitude of the transverse velocity generated by the S_0 mode is much smaller than the A_0 mode, the S_0 mode captured by the LDV is much less sensitive. Therefore in this study only the A_0 mode was chosen for processing the wave signals. At 250 kHz, the phase velocity of the A_0 mode is 1.452 km/s. Using Eq. (4) [22], the optimal angle of excitation, θ, can be calculated

$$\sin\theta = \frac{c}{c_p} \tag{4}$$

where c is the sound velocity in the excitation medium (Air: 343 m/s) and c_p is the phase velocity of the A_0 mode in the plate (1.452 km/s). The resulting optimal angle of excitation for the air-coupled transducer is 13.66 degrees (13.5 degrees was used in the experiment).

The out-of-plane velocity of the wavefield, defined by $w(x,y,t)$, can be assembled from all the time series from the LDV in the scan area. The wavefield is then windowed in time after the actuation is triggered, and prior to the wave reflected back from right edge of the plate. The wavefield $w(x,y,t)$ is plotted at several time steps as a 3-D surface plot (Figure 13) and as a 2-D contour plot (Figure 14).

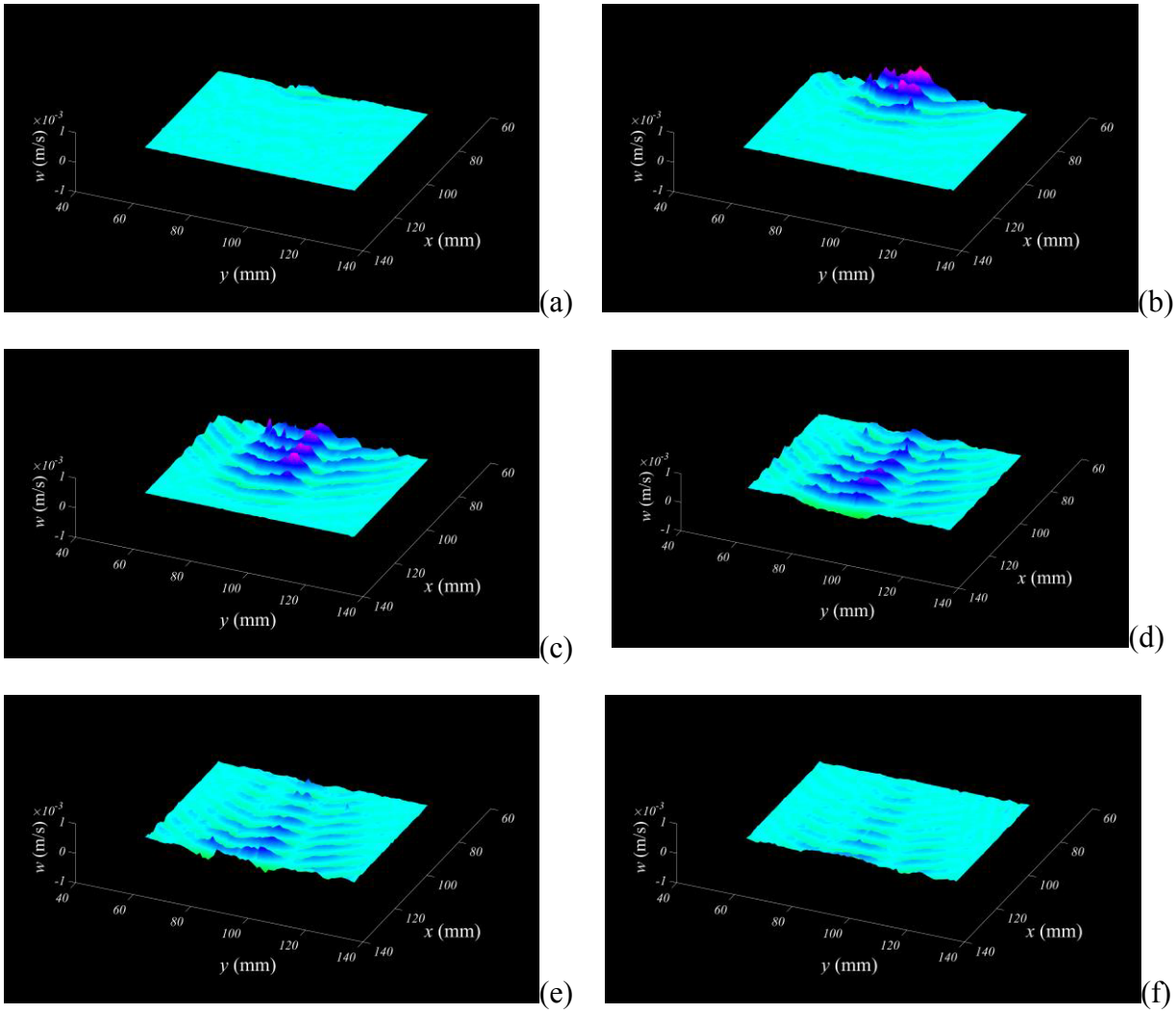

Figure 13. 3-D surface plots of the out-of-plane velocity, $w(x,y,t)$, of wavefield at times (a) 155.9 μs, (b) 165.6 μs, (c) 175.4 μs, (d) 185.2 μs, (e) 194.9 μs, and (f) 204.9 μs.

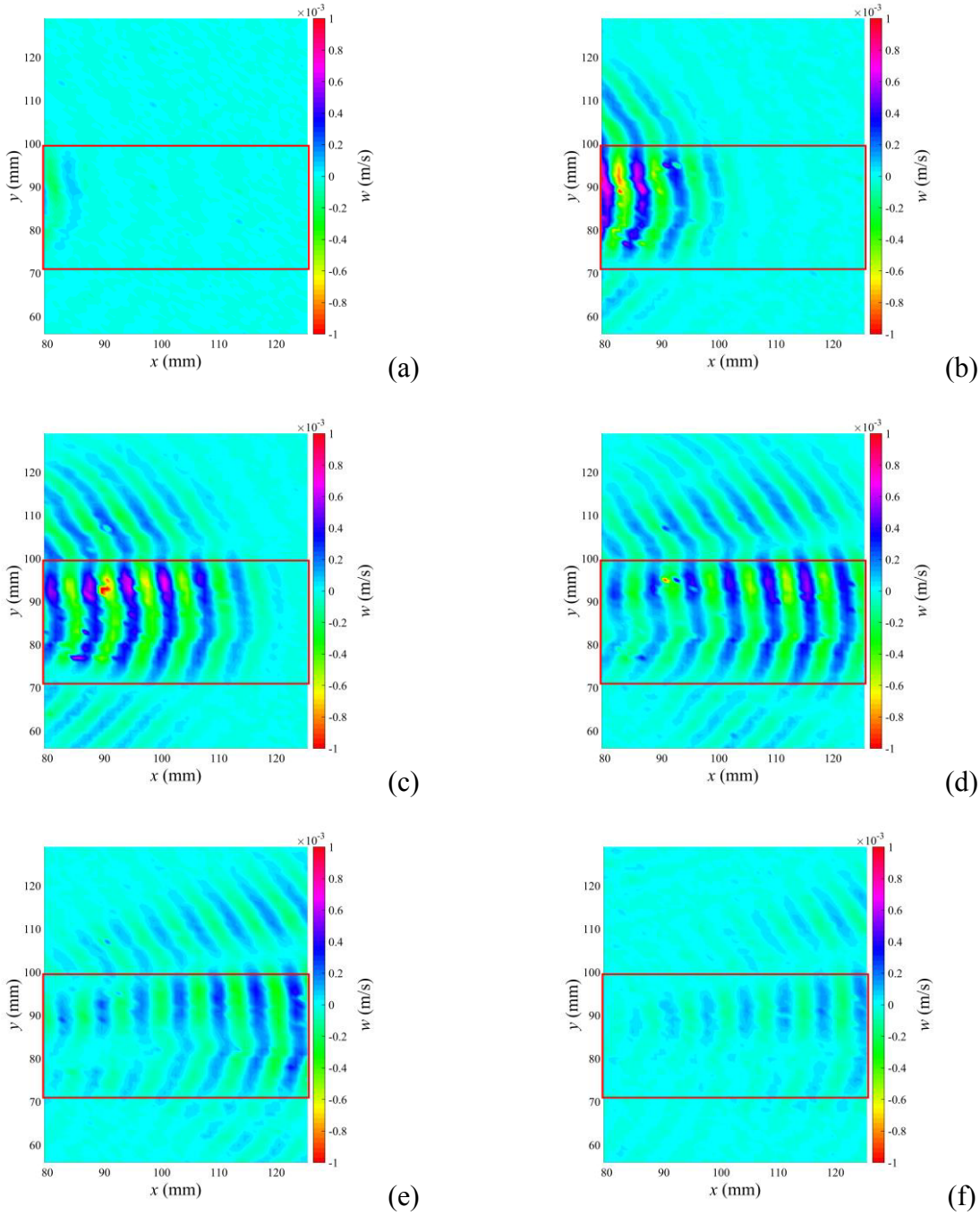

Figure 14. 2-D contour plots of the out-of-plane velocity, $w(x,y,t)$, of wavefield at times (a) 155.9 μs , (b) 165.6 μs , (c) 175.4 μs , (d) 185.2 μs , (e) 194.9 μs , and (f) 204.9 μs in the scan area where the red rectangle outlines the imaged area shown in Figure 6.

The cumulative total wave energy (CTWE) can be calculated by Eq. (5) [19]

$$CTWE(x,y) = \int_{t_i}^{t_f} W^2(x,y,t)\, \mathrm{d}t \tag{5}$$

where t_i is the time at the beginning of the time window measurement and t_f is the time at the end of the time window (prior to the back reflection from right edge of the plate).

CTWE signifies the area illuminated by the air-coupled transducer and serves as a comparison to the area imaged by the ZLCC imaging condition.

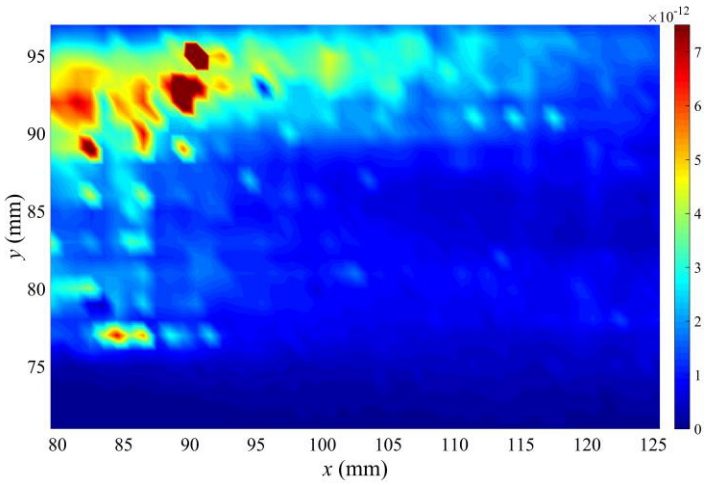

Figure 15. Cumulative total wave energy (CTWE) in the imaged area (outlined by red rectangle shown in Figure 6).

The ZLCC imaging condition for determining the size of the defect is based on the concept that the incident and backscattered wave are in phase on the damage boundaries [20]. From the experimental setup (Figure 5), it can be observed that the incident wave propagates to the right (forward propagating) and the backscattered wave propagates to the left (backward propagating). To decompose $w(x,y,t)$ into the incident and backscatter wave, $w(x,y,t)$ is first transformed from the time-space domain to the frequency-wavenumber domain [19]. This can be accomplished using a two-dimensional Fourier transform (Eq. (6)).

$$\bar{W}(k_x,y,\omega)=\int_{-\infty}^{\infty}\int_{-\infty}^{\infty}w(x,y,t)\mathrm{e}^{-i\left(k_x x-\omega t\right)}\,\mathrm{d}x\,\mathrm{d}t \tag{6}$$

Note the sign convention where a positive k_x denotes a wave propagating forward to the positive (or right) x-direction whereas a negative k_x denotes a wave propagating (scattering back) to the negative (or left) x-direction.

The total wavefield can be readily separated in the frequency-wavenumber domain into the incident $\bar{W}_i(k_x,y,\omega)$ and the backscatter $\bar{W}_{bs}(k_x,y,\omega)$ wave. Both the incident wave and the backscattered wave can be inverted to the frequency-space domain using a one-dimensional spatial Fourier transform (Eq. (7)).

$$W_{i(bs)}\left(x,y,\omega\right)=\tfrac{1}{2\pi}\int_{-\infty}^{\infty}\bar{W}_{i(bs)}\left(k_x,y,\omega\right)\mathrm{e}^{ik_x x}\mathrm{d}x \tag{7}$$

For each measurement location (x_i,y_j), the ZLCC value, $I(x_i,y_j)$, is found using Eq. (8) and Eq. (9) [20]

$$I(x_i, y_j, \omega_k) = W_i(x_i, y_j, \omega_k) W_{bs}^*(x_i, y_j, \omega_k) \tag{8}$$

$$I(x_i, y_j) = \sum_{\omega} I(x_i, y_j, \omega_k) \tag{9}$$

where $W_{bs}^*(x_i, y_j, \omega)$ is the complex conjugate of $W_{bs}(x_i, y_j, \omega)$.

Figure 16 shows the ZLCC value for the imaged area with measurements in a 1 mm x 1 mm grid. The overlap location is denoted by a filled red rectangle below.

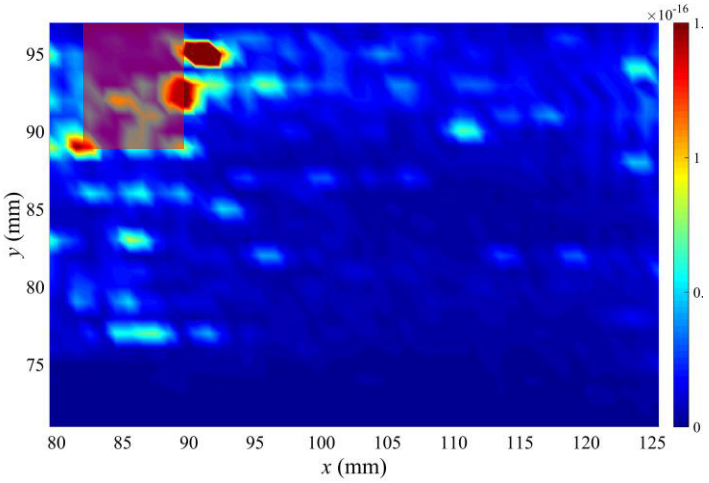

Figure 16. Zero-lag cross-correlation in the imaged area from Figure 6 (overlap location is denoted by the filled red rectangle).

For both Figure 17 and Figure 18, $I(x_i, y_j)$ is calculated with white noise removal at each ω_k step of $I(x_i, y_j, \omega_k)$ before summation. The white noise was mitigated by using a two-dimensional single wavelet transform (Daubechies 10 level 5). The horizontal, vertical, and diagonal details coefficients were calculated using Matlab's Wavelet Toolbox. Figure 17 shows the result when the measurements were taken in a 1 mm × 1 mm grid. Figure 18 shows the result when the measurements were taken in a 2 mm × 2 mm grid. In both figures, the overlap location is denoted by a filled red rectangle.

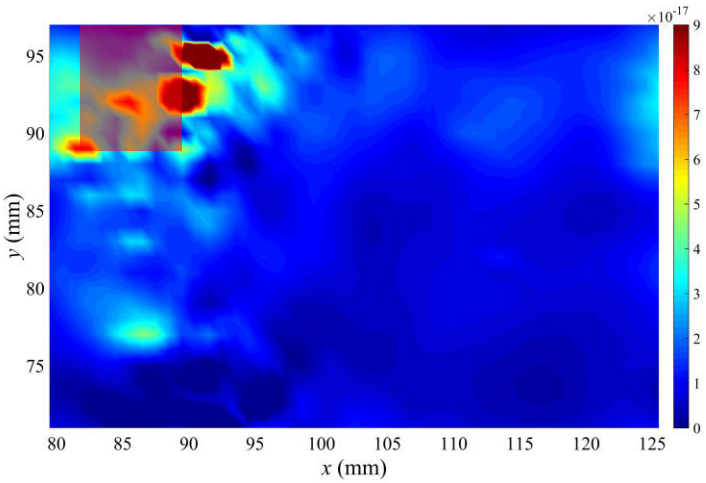

Figure 17. Zero-lag cross-correlation domain with white noise removal at each frequency step before summation in the imaged area from Figure 6 (overlap location is denoted by the filled red rectangle).

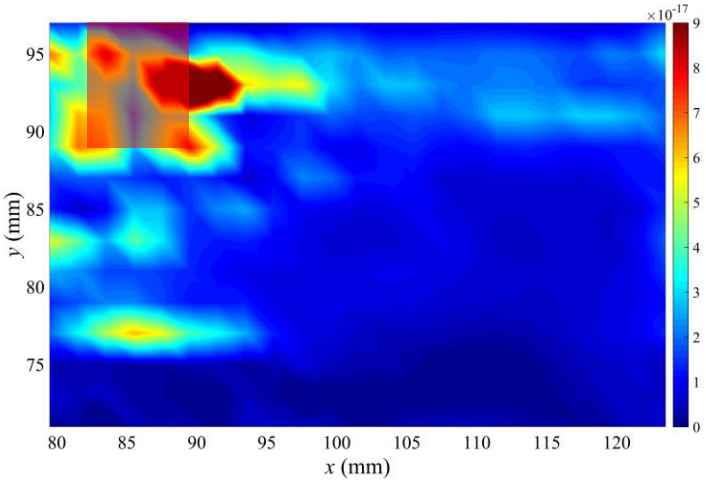

Figure 18. Zero-lag cross-correlation domain with white noise removal at each frequency step before summation in the imaged area from Figure 6 (overlap location is denoted by the filled red rectangle).

The ZLCC imaging condition was utilized to estimate the overlap region within the imaged area up to a 2 mm × 2 mm grid size. Using a two-dimensional single wavelet transform (Daubechies 10 level 5) to mitigate the noise from the image leads to a sharpened image of the overlap location and reduces the presence of false-positives. From Figure 17 and Figure 18, one can notice that the imaged region was biased toward the right side of the overlap region. A possible reason for this outcome is that the wave is traveling from left to right with all of its energy in the original twelve layers. At the left boundary, two prepreg layers are added in the ninety-degree direction (perpendicular to wave propagation direction) causing some degree of the waves reflected (or scattered). However, higher backscattered waves are induced at the right boundary of the overlap where two of the original prepreg layers are suddenly dropped.

The accuracy of the result is limited by following factors. First, the actuation frequency is limited by the response sensitivity of the LDV. If a higher frequency could be measured, then the propagating wave would have a smaller wavelength leading to a greater interaction with the overlap. Second, only a single excitation source location was used. The excitation source could be moved up/down the plate surface and a similar imaged area scanned. The results could then be superimposed to further highlight the overlap region. Finally, the A_0 mode is a flexural mode; therefore, the stress is at a minimum at the neutral axis of the plate. This causes the wave interaction with the overlap to be minimized when the overlap location is at the center of the plate compared to any other location through the thickness.

4. SUMMARY OF RESULTS AND CONCLUSIONS

Three 24-ply unidirectional composite panels were fabricated using a vacuum press where each subsequent panel had a higher final degree of cure and expected lower porosity level than the previous one by varying the cure cycle. Guided waves were propagated and recorded in a pitch-catch configuration normal to the fiber direction using piezoelectric actuators and sensors (Figure 2 and Figure 3). From the group velocity calculated from the actuator-sensor pairs, the average group velocity was determined. The average group velocity increased from 1.53 km/s to 1.62 km/s to 1.64 km/s from Panel #1 to Panel #2 to Panel #3 (Figure 9). Thus, the group velocity of a guided wave may have the potential to serve as an initial index for estimating the degree of cure and level of porosity with further work including micrographs and acid digestion.

Ultimately, the future work will be to fully transition to an in-line detection system that will be able to monitor the degree of cure and porosity in real-time within a part based on group velocity. The in-line detection system will utilize high temperature actuators and sensors for guided wave emission and response detection as well as investigate other metrics such as attenuation of wave energy which will play a critical role during the early stages of cure.

A composite panel with an intentionally introduced overlap in the middle two layers was cured in a vacuum press. A stationary unfocused air-coupled transducer excited a guided wave in the composite plate and a LDV recorded the velocity of the plate in the transverse direction. The response was transformed from the time-space domain to the frequency-wavenumber domain and then separated into the incident and backscatter wave. A zero-lag cross-correlation (ZLCC) imaging condition was proposed to image the overlap region where the incident and backscattered wave are in phase (the boundaries of the overlap). A two-dimensional single wavelet transform was used to mitigate the noise from the ZLCC matrix at each frequency step before summation. The location of the overlap was identified within the imaged area with a grid size up to a 2 mm × 2 mm (Figure 17 and Figure 18).

The future work concerning this detection system will be to mitigate/modify the factors identified in Section 3.2 to sharpen the image within the constraints of the equipment and extend the technique for the detection and size determination of other composite manufacturing defects including gaps, discrete locations of high porosity, voids, through-the-thickness fiber waviness, and in-plane fiber waviness.

5. REFERENCES

1. Hou, T., "Cure cycle design methodology for fabricating reactive resin matrix fiber reinforced composites: A protocol for producing void-free quality laminates." *NASA TM 2014-218524* (2014).
2. Birt, E. & Smith, R., "A review of NDE methods for porosity measurement in fibre-reinforced polymer composites." *Insight-Non-Destructive Testing and Condition Monitoring* 46 (2004): 681-686.
3. Lindrose, A. M., "Ultrasonic wave and moduli changes in a curing epoxy resin." *Experimental Mechanics* 18 (1978): 227-232.
4. Speake, J., Arridge, R. & Curtis, G., "Measurement of the cure of resins by ultrasonic techniques." *Journal of Physics D: Applied Physics* 7 (1974): 412.
5. Adams, R. & Cawley, P., "A review of defect types and nondestructive testing techniques for composites and bonded joints." *NDT international* 21 (1988): 208-222.
6. Stone, D. & Clarke, B., "Ultrasonic attenuation as a measure of void content in carbon-fibre reinforced plastics." *Non-destructive testing* 8 (1975): 137-145.
7. Chen, J., Hoa, S., Jen, C. & Wang, H., "Fiber-optic and ultrasonic measurements for in-situ cure monitoring of graphite/epoxy composites." *Journal of Composite Materials* 33 (1999): 1860-1881.
8. Maffezzoli, A., Quarta, E., Luprano, V., Montagna, G. & Nicolais, L., "Cure monitoring of epoxy matrices for composites by ultrasonic wave propagation." *Journal of Applied Polymer Science* 73 (1999): 1969-1977.
9. Lionetto, F., Tarzia, A. & Maffezzoli, A., "Air-coupled ultrasound: a novel technique for monitoring the curing of thermosetting matrices." *Ultrasonics, Ferroelectrics and Frequency Control, IEEE Transactions on* 54 (2007): 1437-1444.
10. Liebers, N., Raddatz, F. & Schadow, F. *Effective and flexible ultrasound sensors for cure monitoring for industrial composite production.* Deutsche Gesellschaft für Luft-und Raumfahrt-Lilienthal-Oberth eV, 2013.
11. Jeong, H. & Hsu, D., "Experimental analysis of porosity-induced ultrasonic attenuation and velocity change in carbon composites." *Ultrasonics* 33 (1995): 195-203.
12. Pavlopoulou, S., Soutis, C. & Staszewski, W., "Cure monitoring through time-frequency analysis of guided ultrasonic waves." *Plastics, Rubber and Composites* 41 (2012): 4-5.
13. Louie M. & Yuan F. G., "Composite defects from automated fiber placement." *To be Presented at SAMPE Baltimore 2015.* Baltimore, MD, May 18-21, 2015.
14. Croft, K., Lessard, L., Pasini, D., Hojjati, M., Chen, J. & Yousefpour, A., "Experimental study of the effect of automated fiber placement induced defects on performance of composite laminates." *Composites Part A: Applied Science and Manufacturing* 42 (2011): 484-491.
15. Rudberg, T. & Cemenska, J., "Incorporation of laser projectors in machine cell controller reduces ply boundary inspection time, on-part course identification and part probing." *SAE Int.J.Aerosp* 5 (2012): 74-78.
16. Belhaj, M., Deleglise, M., Comas-Cardona, S., Demouveau, H., Binetruy, C., Duval, C. & Figueiredo, P., "Dry fiber automated placement of carbon fibrous preforms." *Composites Part B: Engineering* 50 (2013): 107-111.

17. Schmidt, C., Schultz, C., Weber, P. & Denkena, B., "Evaluation of eddy current testing for quality assurance and process monitoring of automated fiber placement." *Composites Part B: Engineering* 56 (2014): 109-116.
18. Ruzzene, M., "Frequency–wavenumber domain filtering for improved damage visualization." *Smart Materials and Structures* 16 (2007): 2116.
19. An, Y., Park, B. & Sohn, H., "Complete noncontact laser ultrasonic imaging for automated crack visualization in a plate." *Smart Materials and Structures* 22 (2013): 025022.
20. Zhu, R., Huang, G. & Yuan, F. G., "Fast damage imaging using the time-reversal technique in the frequency–wavenumber domain." *Smart Materials and Structures* 22 (2013): 075028.
21. Sohn, H., Park, G., Wait, J. R., Limback, N. P. & Farrar, C. R., "Wavelet-based active sensing for delamination detection in composite structures." *Smart Materials and Structures* 13 (2004): 153-160.
22. Harb, M. & Yuan, F. G., "A rapid, fully non-contact, hybrid system for generating Lamb wave dispersion curve." *Ultrasonics* (Submitted Oct. 2014).